

Lattice Codes for CRYSTALS-Kyber

Shuiyin Liu^{1*} and Amin Sakzad²

^{1*}Cyber Security Research and Innovation Centre, Holmes Institute,
Melbourne, VIC 3000, Victoria, Australia.

²Department of Software Systems & Cybersecurity, Monash University,
Melbourne, VIC 3800, Victoria, Australia.

*Corresponding author(s). E-mail(s): SLiu@Holmes.edu.au;
Contributing authors: Amin.Sakzad@monash.edu;

Abstract

This paper describes a constant-time lattice encoder for the National Institute of Standards and Technology (NIST) recommended post-quantum encryption algorithm: Kyber. The first main contribution of this paper is to refine the analysis of Kyber decoding noise and prove that Kyber decoding noise can be bounded by a sphere. This result shows that the Kyber encoding problem is essentially a sphere packing in a hypercube. The original Kyber encoder uses the integer lattice for sphere packing purposes, which is far from optimal. Our second main contribution is to construct optimal lattice codes to ensure denser packing and a lower decryption failure rate (DFR). Given the same ciphertext size as the original Kyber, the proposed lattice encoder enjoys a larger decoding radius, and is able to encode much more information bits. This way we achieve a decrease of the communication cost by up to **32.6%**, and a reduction of the DFR by a factor of up to **2⁸⁵**. Given the same plaintext size as the original Kyber, e.g., **256** bits, we propose a bit-interleaved coded modulation (BICM) approach, which combines a BCH code and the proposed lattice encoder. The proposed BICM scheme significantly reduces the DFR of Kyber, thus enabling further compression of the ciphertext. Compared with the original Kyber encoder, the communication cost is reduced by **24.49%**, while the DFR is decreased by a factor of **2³⁹**. The proposed encoding scheme is a constant-time algorithm, thus resistant against the timing side-channel attacks.

Keywords: Lattices, Encoding, Lattice-based cryptography, Post-quantum cryptography, Module learning with errors

1 Introduction

The currently deployed Internet key exchange protocols use RSA and Elliptic Curve-based public-key cryptography (ECC), which have been proven to be vulnerable to quantum computing attacks. In July 2022, the National Institute of Standards and Technology (NIST) announced that a new post-quantum algorithm, Kyber, will replace current RSA and ECC-based key-establishment algorithms [1]. The NIST draft standard for Kyber was released in August 2023 [2]. However, the quantum resistance of Kyber is achieved at a high communication cost, which refers to the ciphertext expansion rate (CER), i.e., the ratio of the ciphertext size to the plaintext size. Kyber introduces a 24 – 49 times more communication cost compared to ECC-based algorithms, which limits its practical application for resource-constrained devices.

Kyber uses the module learning with errors problem (M-LWE) as its underlying mathematical problem [3]. Different from RSA and ECC, LWE-based encryption schemes, e.g., Kyber [3], Saber [4], and FrodoKEM [5], have a small decryption failure rate (DFR), where the involved parties fail to derive a shared secret key. Meanwhile, a high DFR might allow an adversary to recover the secret key using a number of failed ciphertexts [6]. For Kyber, an attacker can use Grover search to find the ciphertexts with a slightly higher chance of producing a failure [7]. For Saber, D’Anvers and Battaler have shown that the quantum security can be reduced from 172 bits to 145 bits by using a multitarget decryption failure attack [8]. Therefore, LWE-based encryption schemes commonly choose their parameters so that their DFR is small enough to avoid decryption failure attacks. The downside of these settings is an increased CER and a higher computational complexity.

Given a sufficiently small DFR, coding technologies have the potential to significantly reduce the CER of LWE-based encryption schemes. Some recent research models the decryption decoding problem in LWE-based encryption schemes as the decoding problem on additive white Gaussian noise (AWGN) channels [9][10][11]. Coding theory is then applied to improve the import performance parameters of LWE-based approaches, such as security level, DFR, and CER. In [9], a concatenation of BCH and LDPC codes was introduced to NewHope, to reduce the CER by a factor of 12.8%. In [10], a rate-1/2 polar code was applied to Kyber, to reduce the DFR. In [11], Barnes–Wall lattice codes were used in FrodoKEM, to reduce the CER by a factor of up to 6.7%. However, the decoding noise in Kyber contains a large uniform component: Kyber uses a compression function to round the 12-bit ciphertext coefficients to 4-bit (KYBER512/768) or 5-bit (KYBER1024) integers. When decompressed, a 7 or 8-bit (almost) uniform noise will be added to the ciphertext [7]. Coding approaches for the AWGN channel may not be directly applicable to Kyber.

Despite its advantages, coding technologies add an extra decoding step to the LWE-based encryption schemes, which might be vulnerable to side-channel attacks. A side-channel attack aims to gather information through physical channels such timing, power consumption, and electromagnetic emissions. In [12], the authors proposed a timing side-channel attack for BCH code used in the Ring-LWE scheme LAC. The proposed attack can distinguish between valid ciphertexts and failing ciphertexts, by using the fact that the original BCH decoder decodes valid codewords faster than the

codewords that contain errors. However, this attack can be thwarted using a constant-time decoder. For BCH codes, a constant-time decoder was proposed in [13]. For lattice codes, constant-time decoders have been proposed for Barnes–Wall lattice in [11] and Leech lattice in [14]. By eliminating the non-constant time execution in the decoding process, BCH codes, Barnes–Wall lattice codes, and Leech lattice codes are resistant against the timing attacks.

From an implementation perspective, most research focuses on reducing the execution time of Kyber. In [15], the authors proposed a software implementation of Kyber using a NVIDIA QUADRO GV100 graphics card, to increase the throughput for key exchange by 51 times. In [16], the authors presented a pure hardware implementation of Kyber using Xilinx FPGAs, which achieves a maximum speedup of 129 times for key exchange. In [17], the authors proposed a hardware/software co-design implementation of Kyber in hardware-constrained smart meters. However, these implementations did not address the communication energy cost of Kyber. Since most Internet of Things (IoT) devices are battery-powered wireless sensors, energy efficiency is a crucial requirement for these devices. Kyber introduces a 24 – 49 times more communication energy cost compared to current ECC-based algorithms. If Kyber is adopted for the IoT devices, their battery life may be substantially reduced. There is clearly an urgent need to reduce the communication energy cost (i.e., CER) of Kyber.

In this work, we will demonstrate how to reduce the CER and DFR of Kyber. The main contribution of this paper is twofold: first, we show that the Kyber encoding problem is equivalent to the sphere packing in a hypercube. An explicit tail bound on the decoding noise magnitude is derived. This result allows us to upper bound the Kyber decoding noise as a hypersphere. Second, we propose a lattice-based encoder for Kyber, to ensure the densest packing of the noise sphere. Note that the original Kyber encoder uses a scaled integer lattice, which is far from optimal. Our construction is based on Barnes–Wall lattice and Leech lattice since they are denser than the integer lattice and have constant-time optimal decoders. For a fixed ciphertext size compared to Kyber, the proposed lattice encoder reduces the CER by up to 32.6%, and improves the DFR by a factor of up to 2^{85} . For a fixed plaintext size compared to Kyber, e.g., 256 bits, we propose a bit-interleaved coded modulation (BICM) approach, which combines a BCH code and a lattice encoder. Compared with the original Kyber encoder, the CER is reduced by 24.49%, while the DFR is decreased by a factor of 2^{39} . The proposed encoding scheme is a constant-time algorithm, thus resistant against timing attacks.

2 Preliminaries

2.1 Notation

Rings: Let R and R_q denote the rings $\mathbb{Z}[X]/(X^n + 1)$ and $\mathbb{Z}_q[X]/(X^n + 1)$, respectively. The degree n of the monic polynomial is fixed to 256 in Kyber. Matrices and vectors are represented as bold upper-case and lower-case letters, respectively. We use \mathbf{v}^T to represent the transpose of \mathbf{v} . We use the infinity norm $\|\mathbf{v}\|_\infty$ to represent the magnitude of its largest entry.

Sampling and Distribution: For a set \mathcal{S} , we write $s \leftarrow \mathcal{S}$ to denote that s is chosen uniformly at random from \mathcal{S} . If \mathcal{S} is a probability distribution, then this denotes

that s is chosen according to the distribution \mathcal{S} . For a polynomial $f(x) \in R_q$ or a vector of such polynomials, this notation is defined coefficient-wise. We use $\text{Var}(\mathcal{S})$ to represent the variance of the distribution \mathcal{S} . Let x be a bit string and S be a distribution taking x as the input, then $y \sim S := \text{Sam}(x)$ represents that the output y generated by distribution S and input x can be extended to any desired length. We denote $\beta_\eta = B(2\eta, 0.5) - \eta$ as the central binomial distribution over \mathbb{Z} . We denote $\mathcal{N}(\mu, \sigma^2)$ as the continuous normal distribution over \mathbb{R} , with mean μ and variance σ^2 . We denote $\mathcal{U}(a, b)$ as the discrete uniform distribution over \mathbb{Z} , with minimum $a \in \mathbb{Z}$ and maximum $b \in \mathbb{Z}$.

Compress and Decompress: Let $x \in \mathbb{R}$ be a real number, then $\lceil x \rceil$ means rounding to the closet integer with ties rounded up. Let $x \in \mathbb{Z}_q$ and $d \in \mathbb{Z}$ be such that $2^d < q$. We define

$$\begin{aligned} \text{Compress}_q(x, d) &= \lceil (2^d/q) \cdot x \rceil \bmod 2^d, \\ \text{Decompress}_q(x, d) &= \lceil (q/2^d) \cdot x \rceil. \end{aligned} \tag{1}$$

2.2 Kyber: Key Generation, Encryption, and Decryption

Let k, d_u, d_v be positive integer parameters, which are listed in Table 1. Let $\mathcal{M}_{2,n} = \{0, 1\}^n$ denote the message space, where every message $m \in \mathcal{M}_{2,n}$ can be viewed as a polynomial in R with coefficients in $\{0, 1\}$. Consider the public-key encryption scheme $\text{Kyber.CPA} = (\text{KeyGen}; \text{Enc}; \text{Dec})$ as described in Algorithms 1 to 3 [7].

Algorithm 1 $\text{Kyber.CPA.KeyGen}()$: key generation

- 1: $\rho, \sigma \leftarrow \{0, 1\}^{256}$
 - 2: $\mathbf{A} \sim R_q^{k \times k} := \text{Sam}(\rho)$
 - 3: $(\mathbf{s}, \mathbf{e}) \sim \beta_{\eta_1}^k \times \beta_{\eta_1}^k := \text{Sam}(\sigma)$
 - 4: $\mathbf{t} := \mathbf{A}\mathbf{s} + \mathbf{e}$
 - 5: **return** $(pk := (\mathbf{t}, \rho), sk := \mathbf{s})$
-

Algorithm 2 $\text{Kyber.CPA.Enc}(pk = (\mathbf{t}, \rho), m \in \mathcal{M}_{2,n})$

- 1: $r \leftarrow \{0, 1\}^{256}$
 - 2: $\mathbf{A} \sim R_q^{k \times k} := \text{Sam}(\rho)$
 - 3: $(\mathbf{r}, \mathbf{e}_1, e_2) \sim \beta_{\eta_1}^k \times \beta_{\eta_2}^k \times \beta_{\eta_2} := \text{Sam}(r)$
 - 4: $\mathbf{u} := \text{Compress}_q(\mathbf{A}^T \mathbf{r} + \mathbf{e}_1, d_u)$
 - 5: $v := \text{Compress}_q(\mathbf{t}^T \mathbf{r} + e_2 + \lceil q/2 \rceil \cdot m, d_v)$
 - 6: **return** $c := (\mathbf{u}, v)$
-

Algorithm 3 Kyber.CPA.Dec($sk = \mathbf{s}, c = (\mathbf{u}, v)$)

- 1: $\mathbf{u} := \text{Decompress}_q(\mathbf{u}, d_u)$
 - 2: $v := \text{Decompress}_q(v, d_v)$
 - 3: **return** $\text{Compress}_q(v - \mathbf{s}^T \mathbf{u}, 1)$
-

Table 1 Kyber Parameters in [2][7]: plaintext size = 256 bits

	n	k	q	η_1	η_2	d_u	d_v	δ	CER
KYBER512	256	2	3329	3	2	10	4	2^{-139}	24
KYBER768	256	3	3329	2	2	10	4	2^{-164}	34
KYBER1024	256	4	3329	2	2	11	5	2^{-174}	49

2.3 Kyber Decoding Noise

Let n_e be the decoding noise in Kyber. According to [7][10], we can write n_e as

$$\begin{aligned} n_e &= v - \mathbf{s}^T \mathbf{u} - \lceil q/2 \rceil \cdot m \\ &= \mathbf{e}^T \mathbf{r} + e_2 + c_v - \mathbf{s}^T (\mathbf{e}_1 + \mathbf{c}_u), \end{aligned} \quad (2)$$

where $c_v \leftarrow \psi_{d_v}$, $\mathbf{c}_u \leftarrow \psi_{d_u}^k$ are rounding noises generated due to the compression operation. The elements in c_v or \mathbf{c}_u are assumed to be i.i.d. and independent of other terms in (2). For a small d , e.g., $d = d_v$, we can assume that ψ_d follows a discrete uniform distribution [3]:

$$c_v \leftarrow \psi_{d_v} \approx \mathcal{U}(-\lceil q/2^{d_v+1} \rceil, \lceil q/2^{d_v+1} \rceil). \quad (3)$$

Kyber decoding problem can thus be formulated as

$$y = v - \mathbf{s}^T \mathbf{u} = \lceil q/2 \rceil \cdot m + n_e, \quad (4)$$

i.e., given the observation $y \in R_q$, recover the value of m .

From a coding perspective, an interesting question is if we can model (4) as an AWGN channel. Given the values of q and d_v in Table 1, we observe that n_e contains a uniform component c_v with large variance: 3640 for KYBER512/768, and 918.67 for KYBER1024. Therefore, n_e may not follow a normal distribution and hence (4) may not be treated as an AWGN channel.

In Figure 1, we compare the distribution of first coefficient in n_e , denoted as $n_{e,1}$, with the normal distribution using MATLAB function `normplot()`. If the sample data has a normal distribution, then the data points appear along the reference line. With 100,000 samples, we observe that the distribution of $n_{e,1}$ is different from the normal distribution. This result confirms that the AWGN assumption (4) of [10] is not valid.

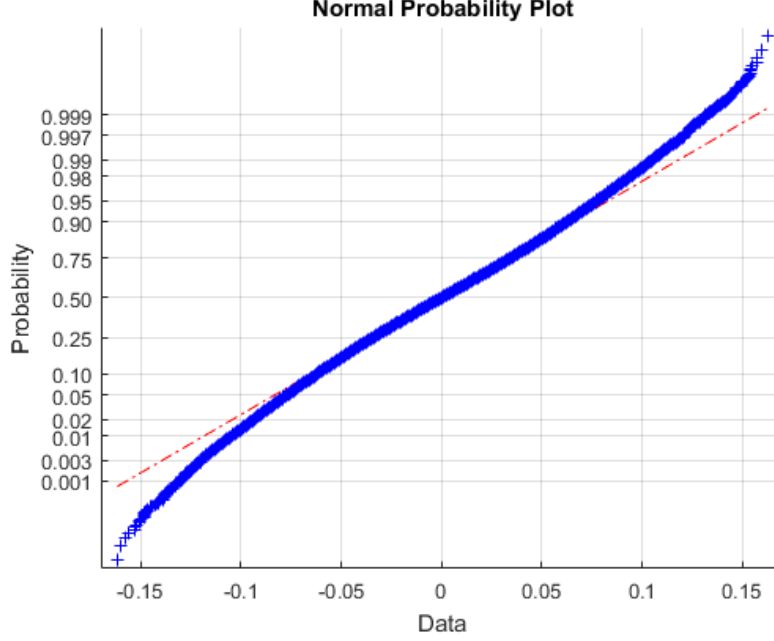


Fig. 1 KYBER768: Comparing the distribution of $n_{e,1}$ to the normal distribution with 100,000 samples.

2.4 Decryption Failure Rate and Ciphertext Expansion Rate

We let $\text{DFR} \triangleq \Pr(\hat{m} \neq m)$, where \hat{m} is the decoded message. Since the original Kyber encodes and decodes m bit-by-bit, DFR can be calculated by [3]:

$$\text{DFR} = \delta := \Pr(\|n_e\|_\infty \geq \lceil q/4 \rceil). \quad (5)$$

Note that it is desirable to have a small δ , e.g., $\delta < 2^{-128}$, in order to be safe against decryption failure attacks [6].

In this work, the communication cost refers to the ciphertext expansion rate (CER),

$$\text{CER} = \frac{\# \text{ of bits in } c}{\# \text{ of bits in } m}, \quad (6)$$

i.e., the ratio of the ciphertext size to the plaintext size. The values of δ and CER are given in Table 1. For comparison purposes, we define the CER reduction ratio as

$$\text{CER-R} \triangleq 1 - \frac{\text{CER}_{\text{reduced}}}{\text{CER}}, \quad (7)$$

where CER represents the original CER of Kyber in Table 1, and $\text{CER}_{\text{reduced}}$ represents the the reduced CER from this work.

3 The Analysis on Kyber Decoding Noise

In this section, we study the distribution of n_e in (2). We will show that n_e can be bounded by a hypersphere.

3.1 The Distribution of n_e

The following lemma considers the product of two central binomial distributed polynomials. It is used to prove Theorem 1, the main result of this section.

Lemma 1. *Suppose that $Z \leftarrow \beta_\eta$ and $Z' \leftarrow \beta_{\eta'}$ are independent, then the polynomial product ZZ' (modulo $X^n + 1$) asymptotically approaches a multivariate normal distribution for large n , i.e.,*

$$ZZ' \leftarrow \mathcal{N}(0, n/4 \cdot \eta\eta' I_n).$$

Proof. The proof is similar to that given in [18, Theorem 3]. To be self-contained, we provide a detailed proof. Let $[Z_0, \dots, Z_{n-1}]^T$ be the coefficients in Z , and $[Z'_0, \dots, Z'_{n-1}]^T$ be the coefficients in Z' . Let $Y = ZZ'$, we have that Y has components $Y_i = \sum_{j=0}^{n-1} \xi(i-j)Z_{i-j}Z'_j$, where $\xi(x) = \text{sign}(x)$ for $x \neq 0$ and $\xi(0) = 1$ [19, p. 338]. Note that $Z_{i-j} = Z_{(i-j) \bmod n}$. The mean of such a component Y_i is given by

$$E(Y_i) = \sum_{j=0}^{n-1} E(\xi(i-j)Z_{i-j}Z'_j) = 0.$$

The summands of a component Y_i are independent, so the variance is given by

$$\text{Var}(Y_i) = \sum_{j=0}^{n-1} \text{Var}(\xi(i-j)Z_{i-j}Z'_j) = n/4 \cdot \eta\eta'. \quad (8)$$

A similar argument shows that covariance of distinct components Y_i and $Y_{i'}$ for $i \neq i'$ is given by

$$\begin{aligned} \text{Cov}(Y_i, Y_{i'}) &= E\left(\sum_{j=0}^{n-1} \xi(i-j)Z_{i-j}Z'_j \cdot \sum_{j'=0}^{n-1} \xi(i'-j')Z_{i'-j'}Z'_{j'}\right) \\ &\quad - \sum_{j=0}^{n-1} E(\xi(i-j)Z_{i-j}Z'_j) \sum_{j'=0}^{n-1} E(\xi(i'-j')Z_{i'-j'}Z'_{j'}) \\ &\stackrel{(a)}{=} (\eta'/2) \cdot \sum_{j=0}^{n-1} \xi(i-j)\xi(i'-j)E(Z_{i-j})E(Z'_{i'-j}) \\ &\quad + (\eta/2) \cdot \sum_{t=0}^{n-1} \xi(i-t)\xi(i'-t)E(Z'_{i-t})E(Z'_{i'-t}) \\ &= 0. \end{aligned} \quad (9)$$

The equality (a) holds since for $(j \neq j', i-j \neq i'-j')$,

$$E(\xi(i-j)Z_{i-j}Z'_j \cdot \xi(i'-j')Z_{i'-j'}Z'_{j'}) = E(\xi(i-j)Z_{i-j}Z'_j) \cdot E(\xi(i'-j')Z_{i'-j'}Z'_{j'}),$$

i.e., $Z_{i-j}, Z'_j, Z_{i'-j'}, Z'_{j'}$ are mutually independent. Therefore, we only need to consider the components with $(j = j', i-j \neq i'-j')$ and $(j \neq j', i-j = i'-j' \bmod n = t)$. We have

$$\text{Cov}(Y_i, Y_{i'}) = \text{Cov}(Y_i, Y_{i'})|_{j=j', i-j \neq i'-j'} + \text{Cov}(Y_i, Y_{i'})|_{j \neq j', i-j = i'-j' \bmod n = t}$$

where

$$\begin{aligned}
& \text{Cov}(Y_i, Y_{i'})|_{j=j', i-j \neq i'-j'} \\
&= E \left(\sum_{j=0}^{n-1} \xi(i-j) \xi(i'-j) Z_{i-j} Z_{i'-j} Z'_j Z'_j \right) \\
&\quad - \sum_{j=0}^{n-1} E \left(\xi(i'-j) Z_{i'-j} Z'_j \right) E \left(\xi(i-j) Z_{i-j} Z'_j \right) \\
&= \sum_{j=0}^{n-1} \left(E \left(Z_j^2 \right) - E \left(Z'_j \right)^2 \right) \xi(i-j) \xi(i'-j) E \left(Z_{i-j} \right) E \left(Z_{i'-j} \right) \\
&= \eta'/2 \sum_{j=0}^{n-1} \xi(i-j) \xi(i'-j) E \left(Z_{i-j} \right) E \left(Z_{i'-j} \right),
\end{aligned}$$

$$\begin{aligned}
& \text{Cov}(Y_i, Y_{i'})|_{j \neq j', i-j = i'-j' \bmod n=t} \\
&= E \left(\sum_{t=0}^{n-1} \xi(i-t) \xi(i'-t) Z_t Z_t Z'_{i-t} Z'_{i-t} \right) \\
&\quad - \sum_{t=0}^{n-1} E \left(\xi(i-t) Z_t Z'_{i-t} \right) E \left(\xi(i'-t) Z_t Z'_{i-t} \right) \\
&= \sum_{t=0}^{n-1} \left(E \left(Z_t^2 \right) - E \left(Z_t \right)^2 \right) \xi(i-t) \xi(i'-t) E \left(Z'_{i-t} \right) E \left(Z'_{i-t} \right) \\
&= \eta/2 \sum_{t=0}^{n-1} \xi(i-t) \xi(i'-t) E \left(Z'_{i-t} \right) E \left(Z'_{i-t} \right).
\end{aligned}$$

According to (8) and (9), $Y = ZZ'$ has covariance matrix $n/4 \cdot \eta\eta' I_n$.

Furthermore, the summands of Y_i are independent and identically distributed, so a Central Limit argument shows that the distribution of Y_i is well-approximated by a normal distribution for large n . Thus Y can be approximated by a multivariate normal distribution. So we have $Y \leftarrow \mathcal{N}(0, n/4 \cdot \eta\eta' I_n)$. \square

Remark 1. Lemma 1 shows the products $\mathbf{e}^T \mathbf{r}$ and $\mathbf{s}^T \mathbf{e}_1$ in (2) asymptotically approach multivariate normal distributions for large n . This result can be easily generalised to the polynomial product of normal and binomial distributions, and two normal distributions as shown in [18].

We then present Theorem 1, and show how it enables us to analyze the DFR and redesign the encoder and decoder for Kyber in the rest of the paper.

Theorem 1. According to the Central Limit Theorem (CLT), the distribution of n_e in (2) asymptotically approaches the sum of multivariate normal and discrete uniform random variables for large n , i.e.,

$$n_e \leftarrow \mathcal{N}(0, \sigma_G^2 I_n) + \mathcal{U}(-\lceil q/2^{d_v+1} \rceil, \lceil q/2^{d_v+1} \rceil), \quad (10)$$

where $\sigma_G^2 = kn\eta_1^2/4 + kn\eta_1/2 \cdot (\eta_2/2 + \text{Var}(\psi_{d_u})) + \eta_2/2$. The values of $\text{Var}(\psi_{d_u})$ are listed in Table 2.

Proof. According to Lemma 1, with $n = 256$, the distribution of $\mathbf{e}^T \mathbf{r}$ in (2) is well-approximated as a multivariate normal distribution, i.e., $\mathbf{e}^T \mathbf{r} \leftarrow \mathcal{N}(0, kn\eta_1^2/4 \cdot I_n)$. Since $e_2 \leftarrow \beta_{\eta_2}$ behaves very similarly to a (discrete) Gaussian and its variance $\eta_2/2$ is much smaller than $kn\eta_1^2/4$, the distribution of $\mathbf{e}^T \mathbf{r} + e_2$ is well-approximated by

$$\mathbf{e}^T \mathbf{r} + e_2 \leftarrow \mathcal{N}(0, (kn\eta_1^2/4 + \eta_2/2) I_n). \quad (11)$$

We then estimate the distribution of $\mathbf{s}^T (\mathbf{e}_1 + \mathbf{c}_u)$. According to [7], the distribution of $\mathbf{e}_1 + \mathbf{c}_u$ behaves very similarly to a Gaussian with the same variance $\eta_2/2 + \text{Var}(\psi_{d_u})$, i.e.,

$$\mathbf{e}_1 + \mathbf{c}_u \leftarrow \mathcal{N}(0, (\eta_2/2 + \text{Var}(\psi_{d_u}))I_n). \quad (12)$$

Using Remark 1, the distribution of $\mathbf{s}^T (\mathbf{e}_1 + \mathbf{c}_u)$ is well-approximated as

$$\mathbf{s}^T (\mathbf{e}_1 + \mathbf{c}_u) \leftarrow \mathcal{N}(0, (kn\eta_1/2 \cdot (\eta_2/2 + \text{Var}(\psi_{d_u})))I_n). \quad (13)$$

Given (11), (13), and (3), for a large n , we can obtain (10). \square

Remark 2. *The idea of Theorem 1 and Lemma 1 is to approximate a discrete normal distribution by a continuous normal distribution. This approximation is commonly used in LWE literature [11][7]. Theorem 1 shows that the coefficients in n_e are independent identically distributed random variables.*

In Table 2, we show the CLT-based noise analysis for Kyber. We consider the normalised noise term $n_e/\lceil q/2 \rceil$ and evaluate its variance. Note that the performance of the best known attacks against LWE-based encryption does not depend on the exact distribution of n_e , but rather on its variance. The values of $\text{Var}(\psi_{d_u})$ are computed numerically as explained in [7]. We observe that the estimated normalised variances match the simulation results.

Table 2 KYBER Decoding Noise Variance
(Normalized): 10,000 samples

	$\text{Var}(\psi_{d_u})$	CLT	Simulation
KYBER512	0.9 [7]	0.0023	0.0023
KYBER768	0.9 [7]	0.0021	0.0021 [10]
KYBER1024	0.38	0.0012	0.0012

In Figure 2, we compare the distribution of the term $\hat{n}_e = \mathbf{e}^T \mathbf{r} + e_2 - \mathbf{s}^T \mathbf{e}_1$ in (2) with the normal distribution using MATLAB function normplot(). This term can be viewed as the *uncompressed* Kyber decoding noise, as $c_v = 0$ and $\mathbf{c}_u = \mathbf{0}$. Theorem 1 shows that for large n ,

$$\hat{n}_e \leftarrow \mathcal{N}(0, (kn\eta_1^2/4 + kn\eta_1\eta_2/4 + \eta_2/2)I_n). \quad (14)$$

With 100,000 samples, we observe that the distribution of the first element in \hat{n}_e , denoted as $\hat{n}_{e,1}$, follows a normal distribution. This result confirms that Theorem 1 is accurate for Kyber with $n = 256$.

3.2 Tail Bound, DFR, and Sphere Packing

To gain more insight, we then estimate the magnitude of n_e based on (10). Without loss of generality, we let

$$n_e^{(\ell)} := [n_{e,1}, n_{e,2}, \dots, n_{e,\ell}]^T$$

to be the ℓ coefficients in n_e , where $1 \leq \ell \leq n$.

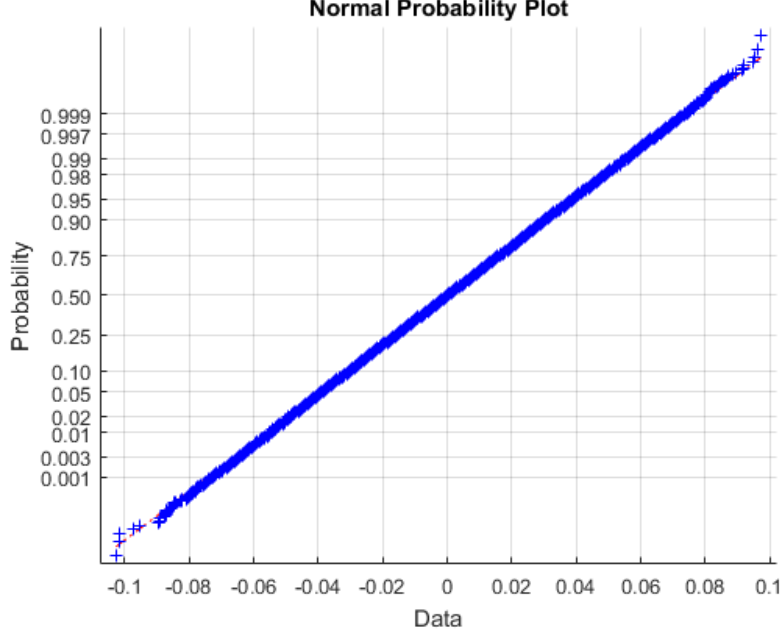


Fig. 2 Uncompressed KYBER768: Comparing the distribution of $\hat{n}_{e,1}$ to the normal distribution with 100,000 samples.

Lemma 2. $\Pr\left(\|n_e^{(\ell)}\| \leq z\right) \geq 1 - Q_{\ell/2}\left(\frac{\sqrt{\ell}\lceil q/2^{d_v+1}\rceil}{\sigma_G}, \frac{z}{\sigma_G}\right)$, for $z \geq 0$, where $Q_M(a, b)$ is the generalised Marcum Q -function.

Proof. Given Theorem 1, we can write $n_{e,i} = x_i + y_i$, where $x_i \leftarrow \mathcal{N}(0, \sigma_G^2)$ and $y_i \leftarrow \mathcal{U}(-\lceil q/2^{d_v+1}\rceil, \lceil q/2^{d_v+1}\rceil)$. Let $\mathbf{y} = [y_1, y_2, \dots, y_\ell]^T$ and $N_U = 2\lceil q/2^{d_v+1}\rceil + 1$. We have

$$\begin{aligned} & \Pr\left(\|n_e^{(\ell)}\| \leq z\right) \\ &= \Pr\left(\sqrt{\sum_{i=1}^{\ell} (x_i + y_i)^2} \leq z\right) \\ &= \sum_{j=1}^{N_U^\ell} \Pr\left(\sqrt{\sum_{i=1}^{\ell} (x_i + \mu_{j,i})^2} \leq z \mid \mathbf{y} = \mu_j\right) \Pr(\mathbf{y} = \mu_j) \\ &= \frac{1}{N_U^\ell} \sum_{j=1}^{N_U^\ell} \Pr\left(\sqrt{\sum_{i=1}^{\ell} (x_i + \mu_{j,i})^2} \leq z \mid \mathbf{y} = \mu_j\right), \end{aligned}$$

where $\mu_j = [\mu_{j,1}, \mu_{j,2}, \dots, \mu_{j,\ell}]^T$ is a sample point in the sample space of \mathbf{y} . Given $y_i = \mu_{j,i}$, $\sqrt{\sum_{i=1}^{\ell} (x_i + \mu_{j,i})^2}$ follows non-central chi distribution, i.e.,

$$\Pr\left(\sqrt{\sum_{i=1}^{\ell} (x_i + \mu_{j,i})^2} / \sigma_G \leq z / \sigma_G \mid \mathbf{y}_j = \mu_j\right) = 1 - Q_{\ell/2}\left(\sqrt{\sum_{i=1}^{\ell} \mu_{j,i}^2} / \sigma_G, z / \sigma_G\right),$$

where $Q_M(a, b)$ is the generalized Marcum Q-function. Since $Q_M(a, b)$ is strictly increasing in a for all $a \geq 0$, we have

$$\begin{aligned} \Pr\left(\|n_e^{(\ell)}\| \leq z\right) &= 1 - \frac{1}{N_U^\ell} \sum_{j=1}^{N_U^\ell} Q_{\ell/2}\left(\sqrt{\sum_{i=1}^{\ell} \mu_{j,i}^2 / \sigma_G^2}, z / \sigma_G\right) \\ &\geq 1 - Q_{\ell/2}\left(\sqrt{\ell} / \sigma_G \cdot \lceil q/2^{d_v+1} \rceil, z / \sigma_G\right). \end{aligned}$$

□

Remark 3. With $\ell = 1$ and $z = \lfloor q/4 \rfloor$, we can easily show

$$\Pr(\|n_{e,1}\| \leq \lfloor q/4 \rfloor) \geq 1 - 2Q\left(\left(\lfloor q/4 \rfloor - \lceil q/2^{d_v+1} \rceil\right) / \sigma_G\right),$$

where $Q(a)$ is the Q-function. It gives an explicit upper bound on the DFR of the original Kyber encoder in (5):

$$\delta \leq 1 - \left(1 - 2Q\left(\left(\lfloor q/4 \rfloor - \lceil q/2^{d_v+1} \rceil\right) / \sigma_G\right)\right)^n.$$

We have $\delta \leq 2^{-142}, 2^{-167}, 2^{-176}$, for KYBER512/768/1024, respectively. Note that the values of δ in Table 1 are evaluated numerically in [3][7]. No closed-form expression is provided.

Lemma 2 shows that Kyber decoding noise $n_e^{(\ell)}$ can be bounded with probability $1 - Q_{\ell/2}\left(\sqrt{\ell} \lceil q/2^{d_v+1} \rceil / \sigma_G, z / \sigma_G\right)$ by a hypersphere with radius z . Since the addition in (4) is over the modulo q domain, we can view the Kyber encoding problem as a sphere packing problem: an arrangement of non-overlapping spheres within a hypercube \mathbb{Z}_q^ℓ . The original Kyber uses the lattice codes $\lfloor q/2 \rfloor \mathbb{Z}_2^\ell$ for sphere packing purposes, which is far from optimal. Even for very small dimensions ℓ , there exist much denser lattices that maintain the same minimal distance between points. In the next section, we will construct lattice codes with denser packing and lower DFR.

4 Lattice Codes for Kyber

4.1 Lattice Codes, Hypercube Shaping, and CVP Decoding

Definition 1 (Lattice). An ℓ -dimensional lattice Λ is a discrete additive subgroup of \mathbb{R}^m , $m \leq \ell$. Based on ℓ linearly independent vectors b_1, \dots, b_ℓ in \mathbb{R}^m , Λ can be written as

$$\Lambda = \mathcal{L}(\mathbf{B}) = z_1 \mathbf{b}_1 + \dots + z_\ell \mathbf{b}_\ell,$$

where $z_1, \dots, z_\ell \in \mathbb{Z}$, and $\mathbf{B} = [\mathbf{b}_1, \dots, \mathbf{b}_\ell]$ is referred to as a generator matrix of Λ .

Definition 2 (Lattice Code). A lattice code $\mathcal{C}(\Lambda, \mathcal{P})$ is the finite set of points in Λ that lie within the region \mathcal{P} :

$$\mathcal{C}(\Lambda, \mathcal{P}) = \Lambda \cap \mathcal{P}.$$

If $\mathcal{P} = \mathbb{Z}_p^\ell$, the code $\mathcal{C}(\Lambda, \mathbb{Z}_p^\ell)$ is said to be generated from hypercube shaping (HS).

Definition 3 (CVP Decoder). Given an input $\mathbf{y} \in \mathbb{R}^\ell$, the Closest Vector Problem (CVP) decoder returns the closest lattice vector to \mathbf{y} over the lattice $\mathcal{L}(\mathbf{B})$, i.e.,

$$\mathbf{x} = \text{CVP}(\mathbf{y}, \mathcal{L}(\mathbf{B})) = \arg \min_{\mathbf{x}' \in \mathcal{L}(\mathbf{B})} \|\mathbf{x}' - \mathbf{y}\|.$$

Definition 4 (HS Encoder [11]). Considering the Smith Normal Form factorization (SNF) of a lattice basis \mathbf{B} , denoted as $\mathbf{B} = \mathbf{U} \cdot \text{diag}(\pi_1, \dots, \pi_\ell) \cdot \mathbf{U}'$, where $\mathbf{U}, \mathbf{U}' \in \mathbb{Z}^{\ell \times \ell}$ are unimodular matrices. Let the message space be

$$\mathcal{M}_{p,\ell} = \{0, 1, \dots, p/\pi_1 - 1\} \times \dots \times \{0, 1, \dots, p/\pi_\ell - 1\}, \quad (15)$$

where $p > 0$ is a common multiplier of π_1, \dots, π_ℓ . Given $\mathbf{m} \in \mathcal{M}_{p,\ell}$, a HS encoder returns a codeword $\mathbf{x} \in \mathcal{C}(\mathcal{L}(\mathbf{B}), \mathbb{Z}_p^\ell)$:

$$\mathbf{x} = \hat{\mathbf{B}}\mathbf{m} \bmod p, \quad (16)$$

where $\hat{\mathbf{B}} = \mathbf{U} \cdot \text{diag}(\pi_1, \dots, \pi_\ell)$.

Definition 5 (HS-CVP Decoder [11]). Let \mathbf{y} be a noisy version of $\mathbf{x} \in \mathcal{C}(\mathcal{L}(\mathbf{B}), \mathbb{Z}_p^\ell)$. The HS-CVP decoder returns an estimated message $\hat{\mathbf{m}} = [\hat{m}_1, \dots, \hat{m}_\ell]^T \in \mathcal{M}_{p,\ell}$:

$$\begin{aligned} \hat{\mathbf{m}} &= \text{HS-CVP}(\mathbf{y}, \mathcal{L}(\hat{\mathbf{B}})) \\ &= \hat{\mathbf{B}}^{-1} \cdot \text{CVP}(\mathbf{y}, \mathcal{L}(\hat{\mathbf{B}})) \bmod (p/\pi_1, \dots, p/\pi_\ell), \end{aligned} \quad (17)$$

where $\hat{m}_i = (\hat{\mathbf{B}}^{-1} \text{CVP}(\mathbf{y}, \mathcal{L}(\hat{\mathbf{B}})))_i \bmod p/\pi_i$, for $i = 1, \dots, \ell$.

For the choice of $\mathcal{L}(\mathbf{B})$, in this work, we consider Barnes–Wall lattice with $\ell = 16$ (BW16) and Leech lattice with $\ell = 24$ (Leech24)[20]. They provide the optimal packing in the corresponding dimensional space and have constant-time CVP decoders [11][14]. Since the coefficients in Kyber are integers, we will scale the original generator matrix to an integer matrix $\mathbf{B} \in \mathbb{Z}^{\ell \times \ell}$, and use the corresponding $\hat{\mathbf{B}}$.

Example 1. For BW16, the matrix \mathbf{B} is given by [11]

$$\mathbf{B} = \begin{bmatrix} 1 & 1 & 1 & 1 & 1 & 2 & 2 & 2 & 2 & 2 & 2 & 2 & 2 & 2 & 2 & 4 \\ 1 & 1 & 1 & 1 & 0 & 2 & 2 & 0 & 2 & 0 & 0 & 2 & 0 & 0 & 0 & 0 \\ 1 & 1 & 1 & 0 & 1 & 2 & 0 & 2 & 0 & 2 & 0 & 0 & 2 & 0 & 0 & 0 \\ 1 & 1 & 1 & 0 & 0 & 2 & 0 & 0 & 0 & 0 & 0 & 0 & 0 & 0 & 0 & 0 \\ 1 & 1 & 0 & 1 & 1 & 0 & 2 & 2 & 0 & 0 & 2 & 0 & 0 & 2 & 0 & 0 \\ 1 & 1 & 0 & 1 & 0 & 0 & 2 & 0 & 0 & 0 & 0 & 0 & 0 & 0 & 0 & 0 \\ 1 & 1 & 0 & 0 & 1 & 0 & 0 & 2 & 0 & 0 & 0 & 0 & 0 & 0 & 0 & 0 \\ 1 & 1 & 0 & 0 & 0 & 0 & 0 & 0 & 0 & 0 & 0 & 0 & 0 & 0 & 0 & 0 \\ 1 & 0 & 1 & 1 & 1 & 0 & 0 & 0 & 2 & 2 & 2 & 0 & 0 & 0 & 2 & 0 \\ 1 & 0 & 1 & 1 & 0 & 0 & 0 & 0 & 2 & 0 & 0 & 0 & 0 & 0 & 0 & 0 \\ 1 & 0 & 1 & 0 & 1 & 0 & 0 & 0 & 0 & 2 & 0 & 0 & 0 & 0 & 0 & 0 \\ 1 & 0 & 1 & 0 & 0 & 0 & 0 & 0 & 0 & 0 & 0 & 0 & 0 & 0 & 0 & 0 \\ 1 & 0 & 0 & 1 & 1 & 0 & 0 & 0 & 0 & 0 & 2 & 0 & 0 & 0 & 0 & 0 \\ 1 & 0 & 0 & 1 & 0 & 0 & 0 & 0 & 0 & 0 & 0 & 0 & 0 & 0 & 0 & 0 \\ 1 & 0 & 0 & 0 & 1 & 0 & 0 & 0 & 0 & 0 & 0 & 0 & 0 & 0 & 0 & 0 \\ 1 & 0 & 0 & 0 & 0 & 0 & 0 & 0 & 0 & 0 & 0 & 0 & 0 & 0 & 0 & 0 \end{bmatrix}. \quad (18)$$

The corresponding matrix $\hat{\mathbf{B}}$ is given by

$$\hat{\mathbf{B}} = \begin{bmatrix} 1 & 0 & 0 & 0 & 0 & 0 & 0 & 0 & 0 & 0 & 0 & 0 & 0 & 0 & 0 & 0 \\ 1 & -1 & 0 & 0 & 0 & 0 & 0 & 0 & 0 & 0 & 0 & 0 & 0 & 0 & 0 & 0 \\ 1 & 0 & -1 & 0 & 0 & 0 & 0 & 0 & 0 & 0 & 0 & 0 & 0 & 0 & 0 & 0 \\ 1 & -1 & -1 & 0 & 0 & 0 & 2 & 2 & 0 & 0 & 0 & 0 & 0 & 0 & 0 & 0 \\ 1 & 0 & 0 & -1 & 0 & 0 & 0 & 0 & 0 & 0 & 0 & 0 & 0 & 0 & 0 & 0 \\ 1 & -1 & 0 & -1 & 0 & 2 & 0 & 0 & 0 & 0 & 0 & 0 & 0 & 0 & 0 & 0 \\ 1 & 0 & -1 & -1 & 0 & 0 & 2 & 0 & 0 & 0 & 0 & 0 & 0 & 0 & 0 & 0 \\ 1 & -1 & -1 & -1 & 0 & 2 & 2 & 2 & 0 & 0 & 0 & 0 & 0 & 0 & 0 & 0 \\ 1 & 0 & 0 & 0 & -1 & 0 & 0 & 0 & 0 & 0 & 0 & 0 & 0 & 0 & 0 & 0 \\ 1 & -1 & 0 & 0 & -1 & 0 & 0 & 0 & 0 & 2 & 0 & 0 & 0 & 0 & 0 & 0 \\ 1 & 0 & -1 & 0 & -1 & 0 & 0 & 0 & 0 & 0 & 2 & 0 & 0 & 0 & 0 & 0 \\ 1 & -1 & -1 & 0 & -1 & 0 & 0 & 2 & 2 & 2 & 2 & -2 & 0 & 0 & 0 & 0 \\ 1 & 0 & 0 & -1 & -1 & 0 & 0 & 0 & 0 & 0 & 2 & -2 & 2 & 0 & 0 & 0 \\ 1 & -1 & 0 & -1 & -1 & 2 & 0 & 0 & 0 & 2 & 2 & -2 & 0 & 2 & 0 & 0 \\ 1 & 0 & -1 & -1 & -1 & 0 & 2 & 0 & 0 & 0 & 2 & 0 & 2 & 0 & 2 & 0 \\ 1 & -1 & -1 & -1 & -1 & 2 & 2 & 2 & 0 & 2 & 2 & -2 & 0 & 2 & 2 & 4 \end{bmatrix}, \quad (19)$$

The values of $\pi_1 \dots \pi_{\ell=16}$ are given by

$$[\pi_1 \dots \pi_{16}] = [1, 1, 1, 1, 1, 2, 2, 2, 2, 2, 2, 2, 2, 2, 2, 4]. \quad (20)$$

4.2 Lattice Encoder and Decoder for Kyber

We divide the n coefficients in m to $\kappa = n/\ell$ blocks:

$$m = [m_{\ell,1}, \dots, m_{\ell,\kappa}]^T \in \mathcal{M}_{p,\ell}^\kappa, \quad (21)$$

where $m_{\ell,i} = [m_{\ell,i,1}, \dots, m_{\ell,i,\ell}]^T \in \mathcal{M}_{p,\ell}$ in (15) is the i^{th} block of coefficients in m , $i = 1, \dots, \kappa$. From the viewpoint of lattice, the model in (4) can be generalized to

$$y = \lceil q/p \rceil \cdot [\hat{\mathbf{B}}m_{\ell,1} \bmod p, \dots, \hat{\mathbf{B}}m_{\ell,\kappa} \bmod p]^T + n_e, \quad (22)$$

where $\hat{\mathbf{B}}$ is given in Definition 4, and $\hat{\mathbf{B}}m_{\ell,i} \bmod p \in \mathcal{C}(\mathcal{L}(\mathbf{B}), \mathbb{Z}_p^\ell)$, for $i = 1, \dots, \kappa$. In other words, the message $m \in \mathcal{M}_{p,\ell}^\kappa$ is encoded to κ lattice points.

We describe the lattice encoder and decoder in Algorithms 4 and 5, where the encoder $\Lambda\text{-Enc}$ takes as the input a message $m \in \mathcal{M}_{p,\ell}^\kappa$ and outputs v (i.e., the second part of the ciphertext), and where the decoder $\Lambda\text{-Dec}$ takes as input a ciphertext (\mathbf{u}, v) and outputs a message.

Algorithm 4 $\Lambda\text{-Enc}(m \in \mathcal{M}_{p,\ell}^\kappa)$: lattice encoder

//Replace Step 5 in **Algorithm 2**

-
- 1: $x_{\ell,i} := \hat{\mathbf{B}} \cdot m_{\ell,i} \bmod p$, $i = 1, \dots, \kappa$
 - 2: $x := [x_{\ell,1}, \dots, x_{\ell,\kappa}]^T$
 - 3: **return** $v := \text{Compress}_q(\mathbf{t}^T \mathbf{r} + e_2 + \lceil q/p \rceil \cdot x, d_v)$
-

Algorithm 5 $\Lambda\text{-Dec}(\mathbf{u}, v)$: lattice decoder

//Replace Step 3 in **Algorithm 3**

-
- 1: $y := v - \mathbf{s}^T \cdot \mathbf{u} = [y_{\ell,1}, \dots, y_{\ell,\kappa}]^T$, where $y_{\ell,i}$ is the i^{th} block of coefficients in y
 - 2: $m_{\ell,i} := \text{HS} - \text{CVP}(y_{\ell,i}/\lceil q/p \rceil, \mathcal{L}(\mathbf{B}))$, $i = 1, \dots, \kappa$
 - 3: **return** $m := [m_{\ell,1}, \dots, m_{\ell,\kappa}]^T$
-

Remark 4. With $\mathcal{L}(\mathbf{B}) = \mathbb{Z}^\ell$, $\hat{\mathbf{B}} = I_\ell$, and $p = 2$, the proposed lattice encoder and decoder reduce to the original ones used in Kyber.

4.3 CER and DFR Reduction

The number of information bits for each block is given by

$$b(\ell, p) = \sum_{i=1}^{\ell} \log_2(p/\pi_i), \quad (23)$$

where π_i is given in Definition 4, for $i = 1, \dots, \ell$. The total number of encrypted bits can be calculated by

$$N = \kappa b(\ell, p). \quad (24)$$

As shown in Step 3 in Algorithm 4, the ciphertext size remains unchanged. The CER-R in (7) can be calculated by:

$$\text{CER-R} = 1 - n/N = 1 - l/b(\ell, p).$$

Let $\lambda(p)$ be the length of a shortest non-zero vector in the lattice $\mathcal{L}(\lfloor q/p \rfloor \mathbf{B})$. The correct decoding radius of HS-CVP decoder is $\lambda(p)/2$. Let δ_i be the decryption failure rate for the i^{th} block of coefficients $m_{\ell, i}$ in (21). Using Lemma 2, we have

$$\delta_i \leq Q_{\ell/2} \left(\sqrt{\ell}/\sigma_G \cdot \lceil q/2^{d_v+1} \rceil, \lambda(p)/(2\sigma_G) \right).$$

According to Theorem 1, the noise elements in (22) are independent from block to block. Therefore, the decryption failure rate of κ blocks can be calculated by

$$\delta = 1 - \prod_{i=1}^{\kappa} (1 - \delta_i) \approx \kappa Q_{\ell/2} \left(\sqrt{\ell}/\sigma_G \cdot \lceil q/2^{d_v+1} \rceil, \lambda(p)/(2\sigma_G) \right). \quad (25)$$

Table 3 compares the normalized correct decoding radius $\lambda(p)/(2 \lfloor q/2 \rfloor)$, CER-R, N , and δ for difference lattices. We observe a tradeoff between CER and DFR from Table 3: a smaller CER requires a larger p , which will reduce the correct decoding radius of $\mathcal{L}(\lfloor q/p \rfloor \mathbf{B})$ accordingly. Interestingly, KYBER1024 enjoys a much lower DFR compared to KYBER512/768. This can be explained by the smallest noise variance in Table 2.

Table 3 Lattice Codes for KYBER

Lattice	\mathbb{Z}^ℓ [7]	BW16	Leech24
p	2	4	8
$\lambda(p)/(2 \lfloor q/2 \rfloor)$	0.5	0.7067	0.7067
$b(\ell, p)/\ell$	1	20/16	36/24
N	256	320	380 ¹
CER-R	0%	20%	32.6%
δ : KYBER512	2^{-139}	2^{-149}	2^{-111}
δ : KYBER768	2^{-164}	2^{-177}	2^{-131}
δ : KYBER1024	2^{-174}	2^{-259}	2^{-226}

¹Since $n = 256 = 10 \times 24 + 16$, we consider 10 Leech24 codewords with $p = 8$ and 1 BW16 codeword with $p = 4$

4.4 Decoding Complexity, Security, and Observation

As shown in (17), the decoding complexity is determined by the CVP decoder for the selected lattice. For BW16 lattice, the running time of the constant-time CVP decoder is proportional to 32ℓ [11]. For the Leech lattice, the CVP decoder requires 3, 595 real operations in the worst case [21]. The constant-time implementation of [21]

adds 34.5% of overhead to the algorithm [14]. The proposed lattice encoder is resistant to the timing side-channel attacks. Since lattice encoder/decoding doesn't affect the M-LWE hardness assumption in Kyber [7], the security arguments remain the same.

5 Reducing CER and DFR with a Fixed Plaintext Size

In the previous section, we have shown that lattice codes can reduce CER by increasing the plaintext size. In many applications, the plaintext size is fixed, e.g., 256 bits. In this section, we will explain how to reduce the CER and DFR of Kyber, with a fixed plaintext size $K = 256$.

5.1 Bit-Interleaved Coded Modulation for Kyber

We propose a bit-interleaved coded modulation (BICM) approach, which combines an error-correcting code and a lattice encoder. The concept of BICM was originally proposed for the Rayleigh fading channel [22]. It combines coding with modulation in a situation where the performance of an error-correcting code depends on its minimum Hamming distance, rather than on the minimum Euclidean distance of the modulation symbols. This is achieved by bit-wise interleaving at the error-correcting encoder output. Since the lattice encoder can be viewed as a form of modulation [11], we can apply error correcting codes combined with lattice encoder, by using the extra $N - K$ bits (enabled by the proposed lattice encoder) as the parity check bits of an error correcting code. The values of N are given in Table 3.

Definition 6 (Bit Mapper and Demapper). *The BICM approach involves bit mapper and demapper, where the former maps binary bits to an integer vector, while the latter performs the inverse operation. Let $b_{\ell,i} \in \mathcal{M}_{2,b(\ell,p)}$ be the bit representation of $m_{\ell,i} \in \mathcal{M}_{p,\ell}$ in (21), for $i = 1, \dots, \kappa$. The bit mapper $\mathcal{M}_{2,b(\ell,p)} \mapsto \mathcal{M}_{p,\ell}$ and demapper $\mathcal{M}_{p,\ell} \mapsto \mathcal{M}_{2,b(\ell,p)}$ are defined by*

$$\begin{aligned} \text{bit2int}(b_{\ell,i}) &= m_{\ell,i} = [m_{\ell,i,1}, \dots, m_{\ell,i,\ell}]^T \\ \text{int2bit}(m_{\ell,i}) &= b_{\ell,i} = [b_{\ell,i,1}, \dots, b_{\ell,i,b(\ell,p)}]^T, \end{aligned} \quad (26)$$

where the j^{th} element in $m_{\ell,i}$, denoted as $m_{\ell,i,j}$, is converted to the $\log_2(p/\pi_j)$ bits:

$$\left[b_{\ell,i, \sum_{w=1}^{j-1} \log_2(p/\pi_w) + 1}, \dots, b_{\ell,i, \sum_{w=1}^j \log_2(p/\pi_w)} \right]^T,$$

and vice versa, for $j = 1, \dots, \ell$. The value of $b(\ell, p)$ is given in (23), and π_j is given in Definition 4, for $j = 1, \dots, \ell$.

Definition 7 (BCH Code [13]). *The BICM approach involves an error-correcting code. To avoid the timing side-channel attacks, in this work, we choose BCH code, which has a constant-time decoder [13]. Let BCH (N, K) be a BCH code, where $N = \kappa b(\ell, p)$ is the number of encrypted bits in (24), and $K = 256$ represents the number of information bits. The number of correctable errors denoted as t , can be determined*

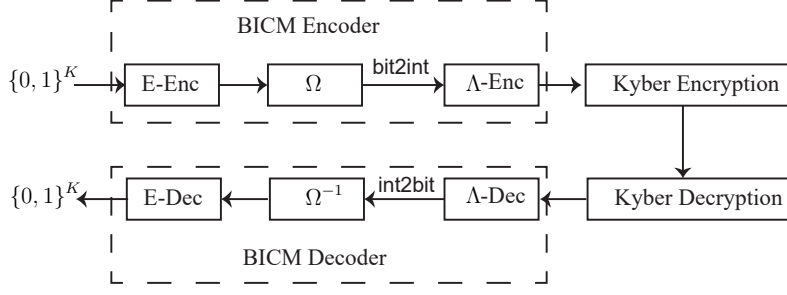


Fig. 3 Block diagram of the proposed bit-interleaved coded modulation.

during the construction of the code. Given a message $m \in \mathcal{M}_{2,K}$, the BCH encoder and decoder are defined by

$$\begin{aligned} [b_{\ell,1}, \dots, b_{\ell,\kappa}]^T &= \text{E-Enc}(m) \\ m &= \text{E-Dec}([b_{\ell,1}, \dots, b_{\ell,\kappa}]^T), \end{aligned} \quad (27)$$

where $b_{\ell,i}$ is defined in (26), for $i = 1, \dots, \kappa$.

Definition 8 (Bit Interleaver and Deinterleaver). *The BICM approach involves bit interleaver and deinterleaver, where the former randomly changes the order of a binary sequence, while the latter performs the inverse operation. The bit interleaver and deinterleaver are defined by*

$$\begin{aligned} [\hat{b}_{\ell,1}, \dots, \hat{b}_{\ell,\kappa}]^T &= \Omega([b_{\ell,1}, \dots, b_{\ell,\kappa}]^T) \\ [b_{\ell,1}, \dots, b_{\ell,\kappa}]^T &= \Omega^{-1}([\hat{b}_{\ell,1}, \dots, \hat{b}_{\ell,\kappa}]^T), \end{aligned} \quad (28)$$

where $b_{\ell,i}$ is defined in (26), and $\hat{b}_{\ell,i}$ represents the permuted bits, for $i = 1, \dots, \kappa$.

Definition 9 (BICM). *The BICM models are represented by the block diagram of Figure 3, which includes 1) an error-correcting code E-Enc in (27); 2) an interleaver Ω in (28); 3) a lattice encoder Λ -Enc in Algorithm 4, modelled by a labelling map $b_{\ell,i}$ in (26) and a lattice point $x_{\ell,i} \in \mathcal{C}(\mathcal{L}(\mathbf{B}), \mathbb{Z}_p^\ell)$, $i = 1, \dots, \kappa$; 4) a lattice decoder Λ -Dec in Algorithm 5; 5) a deinterleaver Ω^{-1} in (28); 6) an error-correcting decoder E-Dec in (27).*

We describe the BICM encoder and decoder in Algorithms 6 and 7, where the encoder BICM-Enc takes as the input a message $m \in \mathcal{M}_{2,K}$ and outputs v (i.e., the second part of the ciphertext), and where the decoder BICM-Dec takes as input a ciphertext (\mathbf{u}, v) and outputs a message.

Algorithm 6 BICM-Enc($m \in \mathcal{M}_{2,\kappa}$): BICM encoder

//Replace Step 5 in **Algorithm 2**

-
- 1: $[b_{\ell,1}, \dots, b_{\ell,\kappa}]^T := \text{E-Enc}(m)$
 - 2: $[\hat{b}_{\ell,1}, \dots, \hat{b}_{\ell,\kappa}]^T := \Omega([b_{\ell,1}, \dots, b_{\ell,\kappa}]^T)$
 - 3: $m_{\ell,i} := \text{bit2int}(\hat{b}_{\ell,i}), i = 1, \dots, \kappa$
 - 4: $x_{\ell,i} := \hat{\mathbf{B}} \cdot m_{\ell,i} \bmod p, i = 1, \dots, \kappa$
 - 5: $x := [x_{\ell,1}, \dots, x_{\ell,\kappa}]^T$
 - 6: **return** $v := \text{Compress}_q(\mathbf{t}^T \mathbf{r} + e_2 + \lfloor q/p \rfloor \cdot x, d_v)$
-

Algorithm 7 BICM-Dec(\mathbf{u}, v): BICM decoder

//Replace Step 3 in **Algorithm 3**

-
- 1: $y := v - \mathbf{s}^T \cdot \mathbf{u} = [y_{\ell,1}, \dots, y_{\ell,\kappa}]^T$, where $y_{\ell,i}$ is the i^{th} block of coefficients in y
 - 2: $m_{\ell,i} := \text{HS} - \text{CVP}(y_{\ell,i}/\lfloor q/p \rfloor, \mathcal{L}(\mathbf{B})), i = 1, \dots, \kappa$
 - 3: $\hat{b}_{\ell,i} := \text{int2bit}(m_{\ell,i}), i = 1, \dots, \kappa$
 - 4: $[b_{\ell,1}, \dots, b_{\ell,\kappa}]^T := \Omega^{-1}([\hat{b}_{\ell,1}, \dots, \hat{b}_{\ell,\kappa}]^T)$
 - 5: **return** $m := \text{E-Dec}([b_{\ell,1}, \dots, b_{\ell,\kappa}]^T)$
-

5.2 CER and DFR Reduction

We now explain how to calculate the DFR for the proposed BICM approach. Let $\text{BER}_i \triangleq \Pr(\hat{b}_i \neq b_i)$ be the *raw* bit error rate for the i^{th} bit, for $i = 1, \dots, N$. Since the interleaver Ω spreads bursts of errors overall N bits in κ blocks, we can assume

$$\text{BER}_1 = \text{BER}_2 = \dots = \text{BER}_N = \text{BER}, \quad (29)$$

and the coded bits go through essentially independent channels. It means that $\delta = 1 - (1 - \text{BER})^N \approx N \cdot \text{BER}$. Therefore, the DFR with BICM, denoted as δ_c , can be computed by

$$\delta_c = \sum_{j=t+1}^N \binom{N}{j} \text{BER}^j (1 - \text{BER})^{N-j} < \sum_{j=t+1}^N \binom{N}{j} \text{BER}^j \approx \binom{N}{t+1} \left(\frac{\delta}{N}\right)^{t+1}, \quad (30)$$

where t is given in Definition 7, N is given in (24), and δ is given in (25).

Considering the value of δ in Table 3, we see that the proposed BICM scheme can significantly reduce the DFR of Kyber for large t . This advantage allows us to reduce the ciphertext size by further compressing the first part of the ciphertext, i.e., \mathbf{u} , since we can afford larger decoding noise. Let \hat{d}_u be the compression parameter for \mathbf{u} used in the BICM approach. The CER reduction ratio for Kyber in (7) can then be

calculated as:

$$\text{CER-R} = 1 - \frac{kn\hat{d}_u + nd_v}{knd_u + nd_v} \leq 1 - \frac{\hat{d}_u}{d_u}, \quad (31)$$

where the values of (n, k, d_u, d_v) are given in Table 1. Note that the value of δ_c in (30) will be calculated based on \hat{d}_u .

Example 2. For BW16 lattice with $p = 4$, we construct a primitive narrow-sense BCH(511, 448) code and then shorten it to (320, 257) by removing the 191 bits of padded 0s [23]. This BCH code generates the codeword out of 256 secret key bits, 63 redundancy bits and 1 padding bit. It can correct $t = 7$ errors. Table 4 compares $(\delta_c, \text{CER-R})$ for difference \hat{d}_u . We observe that the BICM approach can significantly reduce DFR and CER of Kyber.

Table 4 BCH(320, 257)-BW16 for KYBER

	$\hat{d}_u = 9$	$\hat{d}_u = 8$
$\text{Var}(\psi_{d_u})$	3.8	14.1
$(\delta_c, \text{CER-R}): \text{KYBER512}$	$(2^{-623}, 8.33\%)$	$(2^{-194}, 16.67\%)$
$(\delta_c, \text{CER-R}): \text{KYBER768}$	$(2^{-683}, 8.82\%)$	$(2^{-202}, 17.65\%)$
$(\delta_c, \text{CER-R}): \text{KYBER1024}$	$(2^{-791}, 16.33\%)$	$(2^{-213}, 24.49\%)$

5.3 Security

As shown in Table 4, the value of $\text{Var}(\psi_{d_u})$ increases as the value of \hat{d}_u decreases. According to [7], adding more rounding noise will make the M-LWE problem harder. Moreover, the proposed BICM scheme is resistant to timing attacks, as it uses constant-time BCH and lattice decoders.

6 Conclusion

Our analysis has shown that powerful error-correcting codes within the lattice encoder can lead to a significant improvement of important performance parameters of Kyber, such as security level, decryption failure rate, and communication cost. The lattice encoder can be viewed as a form of coded modulation, which ensures denser packing and lower raw bit error rate, while classical codes, e.g., BCH, can be used to get a high error-correcting capability. The proposed BICM approach, i.e., BCH codes through lattice modulation, combines their advantages to achieve a quasi-error-free key exchange with a high error-correcting capability. Through the use of BICM, we have obtained enhanced parameter sets for Kyber, offering higher security levels, smaller decryption failure rates, and smaller communication costs at the same time.

Data Availability Statement

We do not analyse or generate any datasets, because our work proceeds within a theoretical and mathematical approach. One can obtain the relevant materials from the references below.

References

- [1] The NIST PQC Team: PQC standardization process: Announcing four candidates to be standardized, plus fourth round candidates (2022). <https://csrc.nist.gov/News/2022/pqc-candidates-to-be-standardized-and-round-4>
- [2] National Institute of Standards and Technology: Module-Lattice-based Key Encapsulation Mechanism Standard. Federal Information Processing Standards Publication (FIPS) NIST FIPS 203 ipd. (2023) <https://doi.org/10.6028/NIST.FIPS.203.ipd>
- [3] Bos, J., Ducas, L., Kiltz, E., Lepoint, T., Lyubashevsky, V., Schanck, J.M., Schwabe, P., Seiler, G., Stehlé, D.: CRYSTALS - Kyber: A CCA-Secure Module-Lattice-Based KEM. In: 2018 IEEE European Symposium on Security and Privacy (EuroS&P), pp. 353–367 (2018). <https://doi.org/10.1109/EuroSP.2018.00032>
- [4] D’Anvers, J.-P., Karmakar, A., Sinha Roy, S., Vercauteren, F.: Saber: Module-LWR Based Key Exchange, CPA-Secure Encryption and CCA-Secure KEM. In: Joux, A., Nitaj, A., Rachidi, T. (eds.) Progress in Cryptology – AFRICACRYPT 2018, pp. 282–305. Springer, Cham (2018). https://doi.org/10.1007/978-3-319-89339-6_16
- [5] Alkim, E., Bos, J.W., Ducas, L., Longa, P., Mironov, I., Naehrig, M., Nikolaenko, V., Peikert, C., Raghunathan, A., Stebila, D.: FrodoKEM: Learning With Errors Key Encapsulation. NIST Round 3 specification (2021). <https://frodokem.org/>
- [6] D’Anvers, J.-P., Guo, Q., Johansson, T., Nilsson, A., Vercauteren, F., Verbauwhede, I.: Decryption Failure Attacks on IND-CCA Secure Lattice-Based Schemes. In: Lin, D., Sako, K. (eds.) Public-Key Cryptography – PKC 2019, pp. 565–598. Springer, Cham (2019). https://doi.org/10.1007/978-3-030-17259-6_19
- [7] Avanzi, R., Bos, J., Ducas, L., Kiltz, E., Lepoint, T., Lyubashevsky, V., Schanck, J., Schwabe, P., Seiler, G., Stehlé, D.: Algorithm specifications and supporting documentation (version 3.02). Tech. rep., Submission to the NIST post-quantum project (2021). <https://pq-crystals.org/kyber/resources.shtml>
- [8] D’Anvers, J.-P., Batsleer, S.: Multitarget Decryption Failure Attacks and Their Application to Saber and Kyber. In: Hanaoka, G., Shikata, J., Watanabe, Y. (eds.) Public-Key Cryptography – PKC 2022, pp. 3–33. Springer, Cham (2022). https://doi.org/10.1007/978-3-030-97121-2_1

- [9] Fritzmann, T., Pöppelmann, T., Sepulveda, J.: Analysis of error-correcting codes for lattice-based key exchange. In: Cid, C., Jacobson Jr., M.J. (eds.) *Selected Areas in Cryptography – SAC 2018*, pp. 369–390. Springer, Cham (2019). https://doi.org/10.1007/978-3-030-10970-7_17
- [10] Papadopoulos, I., Wang, J.: Polar codes for Module-LWE public key encryption: The case of Kyber. *Cryptography* **7**(1) (2023) <https://doi.org/10.3390/cryptography7010002>
- [11] Lyu, S., Liu, L., Ling, C., Lai, J., Chen, H.: Lattice Codes for Lattice-Based PKE. In: *Des. Codes Cryptogr.* (2023). <https://doi.org/10.1007/s10623-023-01321-6>
- [12] D’Anvers, J.-P., Tiepelt, M., Vercauteren, F., Verbauwhede, I.: Timing Attacks on Error Correcting Codes in Post-Quantum Schemes. In: *Proceedings of ACM Workshop on Theory of Implementation Security Workshop. TIS’19*, pp. 2–9. Association for Computing Machinery, New York, NY, USA (2019). <https://doi.org/10.1145/3338467.3358948>
- [13] Walters, M., Roy, S.S.: Constant-time BCH error-correcting code. In: *2020 IEEE International Symposium on Circuits and Systems (ISCAS)*, pp. 1–5 (2020). <https://doi.org/10.1109/ISCAS45731.2020.9180846>
- [14] Poppelen, A.: Cryptographic decoding of the Leech lattice. *Cryptology ePrint Archive*, Paper 2016/1050 (2016). <https://eprint.iacr.org/2016/1050>
- [15] Gupta, N., Jati, A., Chauhan, A.K., Chattopadhyay, A.: PQC Acceleration Using GPUs: FrodoKEM, NewHope, and Kyber. *IEEE Transactions on Parallel and Distributed Systems* **32**(3), 575–586 (2021) <https://doi.org/10.1109/TPDS.2020.3025691>
- [16] Huang, Y., Huang, M., Lei, Z., Wu, J.: A pure hardware implementation of CRYSTALS-KYBER PQC algorithm through resource reuse. *IEICE Electron. Express* **17**, 20200234 (2020) <https://doi.org/10.1587/elex.17.20200234>
- [17] Costa, V.L.R.D., Camponogara, Â., López, J., Ribeiro, M.V.: The Feasibility of the CRYSTALS-Kyber Scheme for Smart Metering Systems. *IEEE Access* **10**, 131303–131317 (2022) <https://doi.org/10.1109/ACCESS.2022.3229521>
- [18] Costache, A., Curtis, B.R., Hales, E., Murphy, S., Ogilvie, T., Player, R.: On the precision loss in approximate homomorphic encryption. *Cryptology ePrint Archive*, Paper 2022/162 (2022). <https://eprint.iacr.org/2022/162>
- [19] Ding, X., Esgin, M.F., Sakzad, A., Steinfeld, R.: An injectivity analysis of Crystals-Kyber and implications on quantum security. In: *Information Security and Privacy*, pp. 332–351. Springer, Cham (2022). https://doi.org/10.1007/978-3-031-22301-3_17

- [20] Conway, J.H., Sloane, N.J.A.: Sphere Packings, Lattices, and Groups, 3rd edn. Springer, New York (1999). <https://doi.org/10.1007/978-1-4757-6568-7>
- [21] Vardy, A., Be'ery, Y.: Maximum likelihood decoding of the Leech lattice. IEEE Transactions on Information Theory **39**(4), 1435–1444 (1993) <https://doi.org/10.1109/18.243466>
- [22] Caire, G., Taricco, G., Biglieri, E.: Bit-interleaved coded modulation. IEEE Trans. Inf. Theory **44**(3), 927–946 (1998) <https://doi.org/10.1109/18.669123>
- [23] Lin, S., Costello, D.J.: Error Control Coding, Second Edition. Prentice-Hall, Inc., USA (2004)